

Electric Dipole Moment of Top Quark and CP -Violating Asymmetries in $\gamma\gamma \rightarrow t\bar{t}$

P. Poulose and Saurabh D. Rindani

*Theory Group, Physical Research Laboratory,
Ahmedabad - 380 009, India*

Abstract

CP -violating asymmetries due to a possible electric dipole interaction of the top quark in the production and subsequent decay of top quark-top antiquark pair in photon-photon collisions are studied. The asymmetries defined can be used to determine the imaginary part of the electric dipole form factors. A $\gamma\gamma$ collider with photon beams generated from laser back-scattering off electron beams with an integrated geometric luminosity of $20 fb^{-1}$ can put a limit of the order of $10^{-17} e cm$ on the imaginary part of the electric dipole form factor of the top quark if the electron beams have longitudinal polarization and the laser beams have circular polarization.

PACS Numbers: 11.30.Er, 13.40.Em, 14.65.Ha

1 Introduction

Studying CP violation and looking for its signatures at colliders (present and future) is important for various reasons. Apart from the fact that any indication of CP violation outside the K-meson and B-meson systems seen at colliders likely to be operational in the near future will be a clear indication of physics beyond the standard model (SM), the phenomenon of CP violation requires to be understood in greater detail. With the expectation and the eventual discovery of the heavy top quark, [1] there have been many studies on the electric/weak dipole form factor of the top quark and the CP violation it induces [2]-[7]. This includes work on signatures of CP violation in $t\bar{t}$ production at e^+e^- colliders [3]-[6], as well as at hadron colliders [7].

Since synchrotron radiation makes increasing the energy of a circular collider far beyond that of LEP2 prohibitive, future colliders operating at higher energies will have to be linear colliders. In the context of linear colliders, the possibility of photon linear colliders has been discussed in the literature [8, 9]. The hope is that such a collider will be operational in the coming decade. In such colliders an intense low-energy laser beam would be backscattered by a high energy e^+/e^- beam to give a high-energy photon beam. This photon beam could then be made to collide with another photon beam or with another lepton beam. In this article we discuss signals of possible CP violation in the production of a top quark - top antiquark pair

in a photon-photon collider, by examining asymmetries in angular distribution of leptons (anti-leptons) that arise in a semi-leptonic decay of the $t\bar{t}$ pair.

The topic of CP violation in $\gamma\gamma \rightarrow t\bar{t}$ has also elicited interest recently. Anlauf *et al.* [10] and Bernreuther *et al.* [11] have discussed CP violation in a Higgs mediated $\gamma\gamma \rightarrow t\bar{t}$ process where they study triple-product correlations as well as asymmetries. Choi and Hagiwara [12], and Baek *et al.* [13] have studied the effect of the top quark electric dipole form factor (EDFF) in asymmetries in the top distribution in $\gamma\gamma \rightarrow t\bar{t}$ with linearly polarized photon beams.

Here we assume a CP -violating electric-dipole interaction of the top quark, but neglect CP violation in top decay. We consider two asymmetries: the charge asymmetry, which is the asymmetry in the number of leptons and antileptons produced in the decay of the top antiquark and the top quark with a CP -conserving angular cut in the forward and backward directions, and the charge asymmetry combined with the forward-backward asymmetry. In the absence of a cut-off, charge asymmetry becomes the asymmetry in the production rates of t and \bar{t} , which is zero due to charge conservation in the absence of CP violation in top decay. The effect of longitudinal electron beam polarization together with circular laser beam polarization on the asymmetries is also studied. With an integrated geometric luminosity of 20 fb^{-1} and an initial electron beam energy of a few hundreds of GeV, the limit that can be placed on the imaginary part of the top quark EDFF is found to be of the order of $10^{-17} e \text{ cm}$.

The paper is organized as follows. Main features of a photon linear collider will be discussed in the next section (Section 2). In Section 3 we derive expressions for the CP -violating asymmetries. The results and conclusion are contained in Section 4.

2 Features of a $\gamma\gamma$ Collider

In a $\gamma\gamma$ collider, high-energy photons would be produced by Compton backscattering of intense low-energy laser beams off high energy electrons [8]. The energy spectrum of a Compton-scattered photon is given by

$$\begin{aligned} \frac{1}{\sigma_c} \frac{d\sigma_c}{dy} &= f(x, y) \\ &= \frac{2\pi\alpha^2}{\sigma_c x m_e^2} \left[\frac{1}{1-y} + 1 - y - 4r(1-x) - 2\lambda_e \lambda_l r x (2r-1)(2-y) \right]. \end{aligned} \quad (1)$$

Here

$$x = \frac{4E_b\omega_0}{m_e^2} = 15.3 \left(\frac{E_b}{\text{TeV}} \right) \left(\frac{\omega_0}{\text{eV}} \right), \quad (2)$$

where E_b is the electron beam energy, ω_0 is the energy of the laser beam and m_e is the electron mass. y is given in terms of the energy of the scattered photon, ω ($\leq E_b \frac{x}{1+x}$) as

$$y = \frac{\omega}{E_b}$$

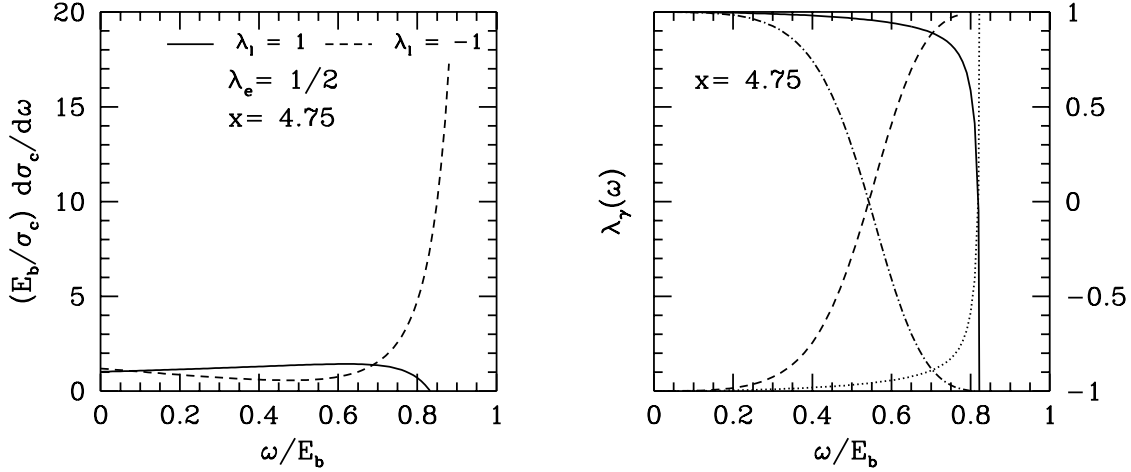


Figure 1: The figure on the left shows the energy distribution of Compton-scattered photons for different helicity combinations of the initial electron beam and the laser beam. In the figure on the right the scattered photon helicity is plotted against the energy of the scattered photon for different helicity combinations of the laser beam and the initial electron beam. Solid and dotted lines correspond to $2\lambda_e\lambda_l = 1$ with $\lambda_e = 1/2$ and $\lambda_e = -1/2$ respectively while the dashed line and the dash-dotted line correspond to $2\lambda_e\lambda_l = -1$ with $\lambda_e = 1/2$ and $\lambda_e = -1/2$, respectively.

and

$$r = \frac{y}{x(1-y)} \leq 1.$$

λ_e and λ_l are the initial electron and laser-photon helicities respectively. Energy distribution in terms of the variable y is related to that in terms of ω , for fixed E_b and ω_0 , by

$$f(\omega) = \frac{1}{\sigma_c} \frac{d\sigma_c}{d\omega} = \frac{1}{E_b} f(x, y). \quad (3)$$

The total cross section σ_c is given by

$$\sigma_c = \sigma_c^{np} + 2\lambda_e\lambda_l\sigma_1,$$

with

$$\sigma_c^{np} = \frac{2\pi\alpha^2}{xm_e^2} \left[\left(1 - \frac{4}{x} - \frac{8}{x^2}\right) \log(x+1) + \frac{1}{2} + \frac{8}{x} - \frac{1}{2(x+1)^2} \right]$$

and

$$\sigma_1 = \frac{2\pi\alpha^2}{xm_e^2} \left[\left(1 + \frac{2}{x}\right) \log(x+1) - \frac{5}{2} + \frac{1}{1+x} - \frac{1}{2(x+1)^2} \right].$$

Here σ_c^{np} is the unpolarized cross section. The energy spectrum $f(x, y)$ plotted against y is shown in Figure 1.

It is clear from the figure that when $\lambda_e\lambda_l < 0$, there are more number of hard photons than soft photons, while for $\lambda_e\lambda_l > 0$ the number of hard photons is less than the number of soft photons. Also in the case of $\lambda_e\lambda_l < 0$ the spectrum peaks at higher energies, resulting in nearly monochromatic beams.

Polarized photon beams are more appropriate for CP violation studies. Dependence of the helicity of the Compton-scattered photon on the energy of the photon is discussed in [8] and is given by

$$\lambda_\gamma(\omega) = \frac{\lambda_l (1 - 2r) (1 - y + \frac{1}{1-y}) + 2\lambda_e r x [1 + (1 - y) (1 - 2r)^2]}{1 - y + \frac{1}{1-y} - 4r (1 - r) - 2\lambda_e \lambda_l r x (2r - 1) (2 - y)}. \quad (4)$$

For $2\lambda_e\lambda_l = -1$, hard photons will have helicity $\lambda = \lambda_e$ (See Figure 1). As already mentioned the number of hard photons is much higher than that of the soft ones at $2\lambda_e\lambda_l = -1$.

Another important aspect of a collider is its luminosity. The luminosity distribution of a $\gamma\gamma$ collider depends on different factors like the conversion distance, *i.e.*, the distance from the scattering point to the interaction point, energy distribution of the beams, etc. Assuming a Gaussian profile for the electron beam with azimuthal symmetry, the luminosity distribution of a $\gamma\gamma$ collider is given in terms of the photon energy distribution by [8]

$$\frac{1}{L_{ee}} \frac{dL_{\gamma\gamma}}{d\omega_1 d\omega_2} = f_1(\omega_1) f_2(\omega_2) I_0 \left(\frac{d_1 d_2}{\sigma_1^2 + \sigma_2^2} \right) e^{-\frac{d_1 d_2}{2(\sigma_1^2 + \sigma_2^2)}}. \quad (5)$$

Here $f_1(\omega_1)$ and $f_2(\omega_2)$ are the energy distributions of the two photon beams (see eqs. (1) and (3)). I_0 is the zeroth order modified Bessel function with $d_i = z_i \theta_{\gamma i}$, where z_i is the conversion distance and $\theta_{\gamma i}$ is the scattering angle of the photon beam, and σ_i is the half width of the Gaussian profile. L_{ee} is the geometric luminosity of the original electron-electron collider. Making a variable change from ω_1 and ω_2 to η and W , where $\eta = \tan^{-1} \left(\frac{\omega_1 - \omega_2}{\omega_1 + \omega_2} \right)$ is the $\gamma\gamma$ rapidity and $W = 2\sqrt{\omega_1 \omega_2}$ is the $\gamma\gamma$ invariant mass, we get the luminosity distribution as

$$\frac{1}{L_{ee}} \frac{dL_{\gamma\gamma}}{dW d\eta} = \frac{W}{2} f_1 \left(\frac{W e^\eta}{2} \right) f_2 \left(\frac{W e^{-\eta}}{2} \right) I_0 \left(\frac{d_1 d_2}{\sigma_1^2 + \sigma_2^2} \right) e^{-\frac{d_1 d_2}{2(\sigma_1^2 + \sigma_2^2)}}. \quad (6)$$

Taking the conversion distance to be zero for simplicity, the expression for the luminosity distribution becomes

$$\frac{1}{L_{ee}} \frac{dL_{\gamma\gamma}}{dW d\eta} = \frac{W}{2} f_1 \left(\frac{W e^\eta}{2} \right) f_2 \left(\frac{W e^{-\eta}}{2} \right). \quad (7)$$

Figure 2 gives the luminosity distribution after rapidity is integrated out. The luminosity peaks at higher values of invariant mass in case of $2\lambda_e\lambda_l = -1$ and the peak value could be as high as 90% of L_{ee} , while for $2\lambda_e\lambda_l = 1$ the spectrum is almost a Gaussian peaking at low energies.

The expression for the number of events in a particular process $\gamma\gamma \rightarrow X$ for the general case of arbitrary electron and laser-photon polarizations is quite complicated. Considerable simplification results with the following assumptions: (i) Axial symmetry of the beam (ii) Only longitudinal polarization of the electron beams (iii) Only circular polarization of the laser beams (iv) Negligible distance between the conversion points and the interaction points. In that case, the converted photons have only circular polarizations given by the average values of the Stokes parameter ξ_2 . The number of events is then given in terms of the luminosity distribution (eq. (7)) and the average value of the Stokes parameters ξ_2 and $\bar{\xi}_2$ of the two photon beams, by [9]

$$dN_{\gamma\gamma \rightarrow X} = dL_{\gamma\gamma} \left(d\sigma_{00} + \xi_2 \bar{\xi}_2 d\sigma_{22} + \xi_2 d\sigma_{20} + \bar{\xi}_2 d\sigma_{02} \right). \quad (8)$$

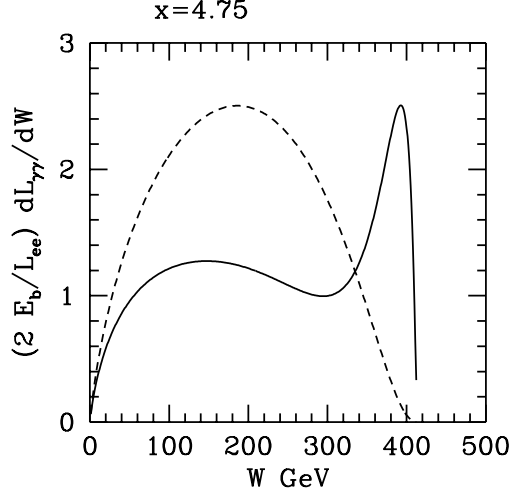


Figure 2: Luminosity distributions are plotted against the $\gamma\gamma$ invariant mass, $W = 2\sqrt{\omega_1\omega_2}$. The initial electron beam energy, E_b is taken to be 250 GeV and a laser beam of energy 1.24 eV is assumed. The solid curve is for $2\lambda_e\lambda_l = -1$ while the dotted curve is for $2\lambda_e\lambda_l = 1$. The conversion distance is assumed to be zero.

Expressions for $d\sigma_{ij}$, which are linear combinations of production density-matrix elements, and ξ_2 and $\bar{\xi}_2$ are given in the appendix.

For large values of L_{ee} , which are possible to achieve, we expect large $t\bar{t}$ production in a $\gamma\gamma$ collider. In the next section we shall discuss some of the CP -violating effects which could be tested in these colliders.

3 Charge Asymmetries in $\gamma\gamma \rightarrow t\bar{t}$

We consider the effective Lagrangian

$$\mathcal{L}_{eff} = \mathcal{L}_{SM} + \mathcal{L}_{CP}, \quad (9)$$

where \mathcal{L}_{SM} is the usual SM Lagrangian, and

$$\mathcal{L}_{CP} = ie d_t \bar{\psi}_t \sigma^{\mu\nu} \gamma_5 \psi_t F_{\mu\nu} \quad (10)$$

with

$$F_{\mu\nu} = \partial_\mu A_\nu - \partial_\nu A_\mu. \quad (11)$$

d_t is the electric dipole form factor and is, in general, complex and momentum dependent. This modifies the SM $t\bar{t}\gamma$ coupling to $ie\Gamma_\mu$, where

$$\Gamma_\mu = \frac{2}{3} \gamma_\mu + d_t \sigma_{\mu\nu} \gamma_5 (p_t + p_{\bar{t}})^\nu. \quad (12)$$

CP violation arising due to this electric dipole moment of the top quark could be studied by using CP -violating asymmetries in the processes involving top-quark coupling with photons. We consider the process $\gamma\gamma \rightarrow t\bar{t}$ with the subsequent decay of t and \bar{t} . We neglect CP violation in the decay of t and \bar{t} .

The asymmetries which do not depend on the top quark momentum that we consider here had been considered by us earlier in the context of an e^+e^- collider [6]. In simple terms these asymmetries are (i) the asymmetry in the number of leptons and antileptons produced as decay products of top antiquark and top quark (the charge asymmetry) and (ii) the sum of the forward-backward asymmetries of the leptons and antileptons. These asymmetries being independent of the top-quark momentum are experimentally favourable. The charge asymmetry is zero in the absence of a cut-off in the polar angle of the lepton (antilepton). This is because when the cut off is zero the charge asymmetry is just the asymmetry in the production rates of t and \bar{t} which is zero from charge conservation assuming that CP is not violated in t decay.

The two asymmetries are written in terms of differential cross section as follows.

$$A_{ch}(\theta_0) = \frac{\int_{\theta_0}^{\pi-\theta_0} d\theta_l \left(\frac{d\sigma^+}{d\theta_l} - \frac{d\sigma^-}{d\theta_l} \right)}{\int_{\theta_0}^{\pi-\theta_0} d\theta_l \left(\frac{d\sigma^+}{d\theta_l} + \frac{d\sigma^-}{d\theta_l} \right)} \quad (13)$$

and

$$A_{fb}(\theta_0) = \frac{\int_{\theta_0}^{\frac{\pi}{2}} d\theta_l \left(\frac{d\sigma^+}{d\theta_l} + \frac{d\sigma^-}{d\theta_l} \right) - \int_{\frac{\pi}{2}}^{\pi-\theta_0} d\theta_l \left(\frac{d\sigma^+}{d\theta_l} + \frac{d\sigma^-}{d\theta_l} \right)}{\int_{\theta_0}^{\pi-\theta_0} d\theta_l \left(\frac{d\sigma^+}{d\theta_l} + \frac{d\sigma^-}{d\theta_l} \right)}. \quad (14)$$

In the above equations, $\frac{d\sigma^+}{d\theta_l}$ and $\frac{d\sigma^-}{d\theta_l}$ refer respectively to the l^+ and l^- distributions in the c.m. frame and θ_0 is the cut-off.

Both the asymmetries defined above are even under naive time reversal T_N , which changes the signs of spins and momenta, without interchange of the initial and final states. They are therefore odd under the combination CPT_N . To avoid conflict with the CPT theorem, the asymmetries can only depend on the imaginary part of d_t .

We consider only the semileptonic decay of $t\bar{t}$. This means that either of t or \bar{t} decays into a b or \bar{b} and leptons, while the other decays hadronically. We choose this semi-leptonic mode for two reasons. Firstly, the leptonic decay (into μ or e) is cleaner to trigger on, and secondly, allowing the other decay to be hadronic gives a larger number of events due to the larger branching ratio. We work in the narrow-width approximation, where W boson is produced on-shell. We also consider on-shell production of t and \bar{t} which allows us to separate the production and decay parts of the amplitude.

The Feynman diagrams for the process $\gamma_\mu(k_1)\gamma_\nu(k_2) \rightarrow t(p_t)\bar{t}(p_{\bar{t}})$ are shown in Figure 3.

We make use of helicity amplitudes. Thus, our approach is different from that of [14], which uses trace techniques, and which was made use of, for example, in [15] in the case of $e^+e^- \rightarrow t\bar{t}$. The production helicity amplitudes are calculated using a method developed by Vega and Wudka [16]. The helicity amplitudes are given by

$$M(\lambda_\gamma, \lambda_\gamma, \lambda_t, \lambda_t) = -\frac{4m_t e^2 Q_t^2}{\sqrt{s}(1 - \beta_t^2 \cos^2 \theta_t)} \{(\lambda_\gamma + \lambda_t \beta_t) - i d_t 2m_t \left[2 + \frac{s}{4m_t^2} \beta_t (\beta_t - \lambda_t \lambda_\gamma) \sin^2 \theta_t \right]\}$$

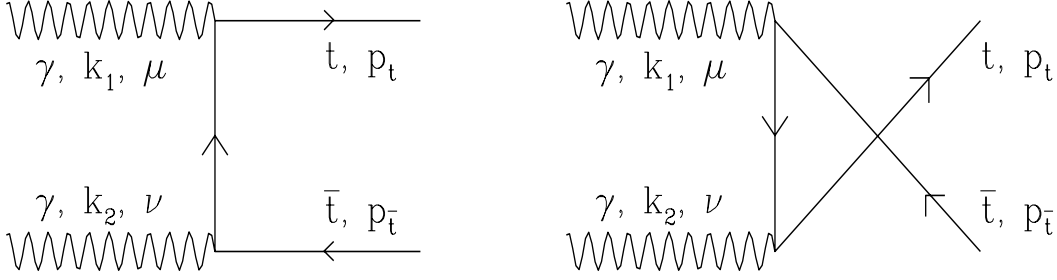


Figure 3: Feynman diagrams for the process $\gamma\gamma \rightarrow t\bar{t}$

$$\begin{aligned}
M(\lambda_\gamma, \lambda_\gamma, \lambda_t, -\lambda_t) &= -\frac{4m_t e^2 Q_t^2}{(1 - \beta_t^2 \cos^2 \theta_t)} \\
&\quad \times \beta_t \sin \theta_t \cos \theta_t \left[\lambda_\gamma i d_t - m_t d_t^2 \right] \\
M(\lambda_\gamma, -\lambda_\gamma, \lambda_t, \lambda_t) &= \frac{4m_t e^2 Q_t^2}{\sqrt{s}(1 - \beta_t^2 \cos^2 \theta_t)} \\
&\quad \times \left[\lambda_t \beta_t + i d_t \frac{s}{2m_t} \beta_t^2 - d_t^2 \frac{s}{2} \lambda_t \beta_t \right] \sin^2 \theta_t \\
M(\lambda_\gamma, -\lambda_\gamma, \lambda_t, -\lambda_t) &= \frac{2\beta_t e^2 Q_t^2}{(1 - \beta_t^2 \cos^2 \theta_t)} \sin \theta_t \left\{ (\lambda_\gamma \lambda_t + \cos \theta_t) \right. \\
&\quad \left. - d_t^2 \frac{s}{2} \left[\frac{4m_t^2}{s} \cos \theta_t + \lambda_\gamma \lambda_t (1 - \beta_t^2 \cos^2 \theta_t) \right] \right\}. \quad (15)
\end{aligned}$$

The notation is that in $M(\lambda_{\gamma_1}, \lambda_{\gamma_2}, \lambda_t, \lambda_{\bar{t}})$, λ_{γ_1} , λ_{γ_2} , λ_t and $\lambda_{\bar{t}}$ correspond to the helicities of the two incoming photons, the top quark and the top antiquark respectively. $Q_t = 2/3$ is the top charge, θ_t is the scattering angle in the c.m. frame, and β_t is the top-quark velocity. It should be noted that d_t occurring in eq. (15) is in reality a dipole form factor and not the on-shell dipole moment, because in Figure 3, one top line at each vertex is off-shell. These expressions agree with those in [13].

To be able to calculate from these amplitudes the differential cross section of the complete process with initial electron states using eq. (8), we first need to know the combinations of cross sections $d\sigma_{ij}$ for the $\gamma\gamma$ subprocess. These we write in terms of the production density matrix elements ρ_{ij} , expressions for which are given in the appendix. We get the following expressions.

$$\begin{aligned}
\frac{d\sigma_{ij}^\pm}{d \cos \theta_t dE_l d \cos \theta_l d\phi_l} &= \frac{3\alpha^2 \beta}{16x_w^2 \sqrt{s}} \frac{E_l}{\Gamma_t \Gamma_W m_W} \left(\frac{1}{1 - \beta \cos \theta_{tl}} - \frac{4E_l}{\sqrt{s}(1 - \beta^2)} \right) \\
&\quad \times \left\{ \left[\rho_{ij}^\pm(++) + \rho_{ij}^\pm(--) \right] (1 - \beta \cos \theta_{tl}) \right. \\
&\quad + \left[\rho_{ij}^\pm(++) - \rho_{ij}^\pm(--) \right] (\cos \theta_{tl} - \beta) \\
&\quad \left. + 2 \operatorname{Re} \left(\rho_{ij}^\pm(+-) \right) (1 - \beta^2) \right\}
\end{aligned}$$

$$\begin{aligned} & \times \sin \theta_t \sin \theta_l (\cos \theta_t \cos \phi_l - \sin \theta_t \cot \theta_l) \\ & + 2 \operatorname{Im} \left(\rho_{ij}^{\pm} (+-) \right) (1 - \beta^2) \sin \theta_t \sin \theta_l \sin \phi_l \}. \end{aligned} \quad (16)$$

Here θ_{tl} is the angle between the top quark and the lepton, and θ_l and ϕ_l are the polar and azimuthal angles of the lepton in the c.m. frame. We consider only terms at most linear in d_t . All the higher-order terms are neglected assuming that d_t is small. The superscript \pm correspond respectively to t and \bar{t} decaying into leptons.

The cross section is given in terms of $d\sigma_{ij}^{\pm}$ as

$$d\sigma^{\pm} = d\sigma_{00}^{\pm} + \xi_2 \bar{\xi}_2 d\sigma_{22}^{\pm} + \xi_2 d\sigma_{20}^{\pm} + \bar{\xi}_2 d\sigma_{02}^{\pm}. \quad (17)$$

We now go over to CP -odd asymmetries which can be obtained from the differential cross section. The charge asymmetry is defined as

$$\begin{aligned} A_{ch} = & \frac{1}{2N} \left\{ \int \frac{dL_{\gamma\gamma}}{d\omega_1 d\omega_2} d\omega_1 d\omega_2 \int_{-1}^1 d \cos \theta_t \right. \\ & \left. \times \int_{\theta_0}^{\pi - \theta_0} d\theta_l \left[\frac{d\sigma^-}{d \cos \theta_t d\theta_l}(\theta_l) - \frac{d\sigma^+}{d \cos \theta_t d\theta_l}(\pi - \theta_l) \right] \right\}. \end{aligned} \quad (18)$$

The charge asymmetry combined with the forward-backward asymmetry is defined as

$$\begin{aligned} A_{fb} = & \frac{1}{2N} \int \frac{dL_{\gamma\gamma}}{d\omega_1 d\omega_2} d\omega_1 d\omega_2 \int_{-1}^1 d \cos \theta_t \\ & \times \left\{ \int_{\theta_0}^{\pi/2} d\theta_l \left[\frac{d\sigma^-}{d \cos \theta_t d\theta_l}(\theta_l) + \frac{d\sigma^+}{d \cos \theta_t d\theta_l}(\pi - \theta_l) \right] \right. \\ & \left. - \int_{\pi/2}^{\pi - \theta_0} d\theta_l \left[\frac{d\sigma^-}{d \cos \theta_t d\theta_l}(\theta_l) + \frac{d\sigma^+}{d \cos \theta_t d\theta_l}(\pi - \theta_l) \right] \right\} \end{aligned} \quad (19)$$

N is the total number of events given by integrating dN in eq. (8) with $d\sigma_{ij}$ given by eq. (16). ω_1 and ω_2 are the energies of the two photon beams.

The expression for the angular distribution given by eq. (16) is in the $\gamma\gamma$ c.m. frame whereas the expressions for A_{ch} and A_{fb} above (eqs. (18) and (19)) are in the lab frame. We will therefore rewrite these latter expressions in the $\gamma\gamma$ c.m. frame. Changing the variable of integration to $\cos \theta_l$ and noticing that the lab frame is obtained by boosting the c.m. frame by a velocity $\beta_\gamma = \frac{\omega_1 - \omega_2}{\omega_1 + \omega_2}$, we get the lower and the upper limits of integration in the $\gamma\gamma$ c.m. frame as

$$f(\theta_0) = \frac{\cos \theta_0^{cm} + \beta_\gamma}{1 + \beta_\gamma \cos \theta_0^{cm}}$$

and

$$\begin{aligned} g(\theta_0) &= \frac{\cos(\pi - \theta_0^{cm}) + \beta_\gamma}{1 + \beta_\gamma \cos(\pi - \theta_0^{cm})} \\ &= \frac{-\cos \theta_0^{cm} + \beta_\gamma}{1 - \beta_\gamma \cos \theta_0^{cm}}. \end{aligned}$$

Making use of the fact that

$$f(\pi - \theta_0) = \frac{-\cos \theta_0^{cm} + \beta_\gamma}{1 - \beta_\gamma \cos \theta_0^{cm}} = g(\theta_0)$$

and

$$g(\pi - \theta_0) = \frac{\cos \theta_0^{cm} + \beta_\gamma}{1 + \beta_\gamma \cos \theta_0^{cm}} = f(\theta_0),$$

we get the final expression for A_{ch} as

$$A_{ch} = \frac{1}{2N} \left\{ \int \frac{dL_{\gamma\gamma}}{d\omega_1 d\omega_2} d\omega_1 d\omega_2 \int_{-1}^1 d \cos \theta_t \right. \\ \left. \times \int_{f(\theta_0)}^{g(\theta_0)} d \cos \theta_l \left[\frac{d\sigma^-}{d \cos \theta_t d \cos \theta_l}(\theta_l) - \frac{d\sigma^+}{d \cos \theta_t d \cos \theta_l}(\theta_l) \right] \right\}, \quad (20)$$

where the differential cross section is in the c.m. frame. A similar expression holds for A_{fb} :

$$A_{fb} = \frac{1}{2N} \int \frac{dL_{\gamma\gamma}}{d\omega_1 d\omega_2} d\omega_1 d\omega_2 \int_{-1}^1 d \cos \theta_t \\ \times \left\{ \int_{f(\theta_0)}^{\beta_\gamma} d \cos \theta_l \left[\frac{d\sigma^-}{d \cos \theta_t d \cos \theta_l}(\theta_l) + \frac{d\sigma^+}{d \cos \theta_t d \cos \theta_l}(\theta_l) \right] \right. \\ \left. - \int_{\beta_\gamma}^{g(\theta_0)} d \cos \theta_l \left[\frac{d\sigma^-}{d \cos \theta_t d \cos \theta_l}(\theta_l) + \frac{d\sigma^+}{d \cos \theta_t d \cos \theta_l}(\theta_l) \right] \right\}. \quad (21)$$

We use the expressions derived above to evaluate the sensitivity of the experimental set-ups with different luminosities and energies to the top dipole moments. The sensitivity of an experiment to the measurement of a physical quantity depends on the statistics. The number of asymmetric events must be greater than the statistical fluctuation by a certain factor for it to be observed. This factor determines the confidence level (C.L.) of the measurement. For a system with one degree of freedom the number of asymmetric events N_A ($= N A$, where A is the asymmetry and N is the total number of events) for a certain value of dipole moment d_t should then be greater than $1.64\sqrt{N}$ for the dipole moment to be observable at the 90% C.L., where \sqrt{N} corresponds to the standard deviation. Using this we can get limits that can be set on the dipole form factors in case the asymmetry is not observed. The 90% C.L. on the dipole form factor is therefore given by

$$\delta d_t = \frac{1.64 d_t}{\sqrt{N A}} = \frac{1.64}{\sqrt{N \mathcal{A}}}, \quad (22)$$

where $\mathcal{A} = A/d_t$ is the value of the asymmetry A for unit dipole moment.

The following section discusses the results we obtain. We have carried out the $\cos \theta_l$ integrals in the above expressions analytically, and the remaining integrals, viz., those over $\cos \theta_t$, ω_1 and ω_2 , numerically.

λ_e^1	λ_e^2	λ_l^1	λ_l^2	N	Asymmetries		Limits on $\text{Im } d_t$ ($10^{-16} e cm$) from	
					A_{ch}	A_{fb}	$ A_{ch} $	$ A_{fb} $
-.5	-.5	-1	-1	76	-.019	0	2.76	
-.5	-.5	1	-1	252	-.025	-.129	1.19	.230
-.5	-.5	1	1	631	-.035	0	.54	
.5	-.5	-1	-1	73	-.024	.013	2.31	4.25
.5	-.5	1	-1	32	-.021	-.080	3.89	1.03
.5	-.5	-1	1	163	-.021	.033	1.73	1.12
Unpolarized				194	-.028	0	1.19	

Table 1: Asymmetries and corresponding 90% C.L. limits obtained on $\text{Im } d_t$ for various combinations of initial beam helicities. The top mass is kept at $m_t = 174$ GeV and an initial electron beam of energy $E_b = 250$ GeV and a laser beam of energy $\omega_0 = 1.24$ eV are assumed. The cut-off angle taken is $\theta_0 = 30^\circ$. N is the total number of events. Asymmetries are for $\text{Im } d_t = \frac{1}{2m_t}$.

4 Results and Conclusion

Charge asymmetry and forward-backward asymmetry combined with charge asymmetry are calculated for different initial-beam helicities. Also, fixing a particular helicity combination, asymmetries are obtained at different electron beam energies and for different laser beam energies. In doing so, the value of x is kept constant. Variation of asymmetries with x , fixing variables like the helicities and cut-off angle is also studied. Asymmetries are also studied at different cut-off angles with beam energy and other parameters kept constant. All the calculations are done assuming a geometrical integrated luminosity of 20 fb^{-1} for the electron-electron collider. We also assume the laser energy ω_0 to be 1.24 eV. We discuss the results in the following.

Table 1 displays asymmetries (in all cases we calculate asymmetries for a fixed value of $\text{Im } d_t = 1/(2m_t)$) obtained for different helicity combinations for beam energy 250 GeV and cut-off angle 30° . The top-quark mass is taken to be 174 GeV. Some important features of the results in Table 1 may be noted. There is no combined asymmetry when both $\lambda_e^1 = \lambda_e^2$ and $\lambda_l^1 = \lambda_l^2$. This is expected as the forward and backward directions cannot be distinguished in this case because the two colliding photons are identical. In SM electromagnetic interactions respect parity and hence the cross section is symmetric under $\lambda_e^i \leftrightarrow -\lambda_e^i$. Thus the total number of events, which gets contribution only from SM, remains the same under this transformation.

As seen from Table 1, the 90% C. L. limits on $\text{Im } d_t$ are in general of the order of $10^{-16} e cm$. The limit obtained on $\text{Im } d_t$ in the unpolarized case is $1.19 \times 10^{-16} e cm$.

E_b (GeV)	N	Asymmetries		Limits on Im d_t ($10^{-16} e cm$) from	
		A_{ch}	A_{fb}	$ A_{ch} $	$ A_{fb} $
250	252	-.025	.129	1.19	.230
500	1441	-.167	.420	.074	.029
750	1210	-.223	.347	.060	.039
1000	996	-.227	.244	.065	.061

Table 2: Variation of limits on Im d_t obtained at different beam energies keeping x fixed at 4.75 (by choosing suitable laser beam energy in each case). The top mass used is 174 GeV and the cut-off angle is taken to be 30° . Asymmetries are for Im $d_t = \frac{1}{2m_t}$. Helicities of the initial electron and laser beams are $\lambda_e^1 = -.5$, $\lambda_e^2 = -.5$, $\lambda_l^1 = -1$ and $\lambda_l^2 = 1$.

Forward-backward combined asymmetry is zero in this case. The best limit obtained is however an order of magnitude better. Its value is $2.3 \times 10^{-17} e cm$ and comes from A_{fb} with initial-beam helicities satisfying $\lambda_e^1 = \lambda_e^2$ and $\lambda_l^1 = -\lambda_l^2$. We consider this helicity combination for further analysis. It may be noted, however, that with unpolarized electron beams and laser beams we can measure only the charge asymmetry.

Table 2 lists the limits for different electron beam energies. The table shows that the limits are better around a beam energy of 500 GeV in the case of combined asymmetry and at around 750 GeV in the case of charge asymmetry. The limit obtained at this value is almost 20 times better than the limit at 250 GeV in the case of charge asymmetry while in the case of combined asymmetry it is a factor of almost 8.

The cut-off angle is also varied to study the variation of limits on Im d_t . The result is tabulated in Table 3. As mentioned before, charge asymmetry, which is the total leptonic charge in the semi-leptonic decay of $t\bar{t}$ is zero when there is no cut-off. Charge asymmetry is found to give best limits on the dipole form factors around a cut-off of 60° whereas the combined asymmetry is better at lower cut-offs.

For a fixed beam energy and at a fixed cut-off angle, variation of Im d_t limits with x is studied in Table 4. From the table it is clear that the limits are better at higher x values. In fact, for x less than about 3, the event rate is quite low, and no significant limit on the dipole moment may be expected. On the other hand, for $x > 4.83$, e^+e^- production due to the collision of high energy photon beam with laser beam is considerable [8]. This introduces additional e^+e^- beam backgrounds as well as degrading the photon spectrum.

To conclude, we find that for an electron beam energy of 250 GeV, and for a suitable choice of circular polarizations of the laser photons and longitudinal polarizations for the electron beams, and assuming a geometrical luminosity of 20 fb^{-1} for the electron beam, it is possible to obtain limits on the imaginary part of the top EDFD of the order of $10^{-17} e cm$. An order of magnitude improvement is possible if the beam energy is increased to 500 GeV. In

θ_0 (deg.)	N	Asymmetries		Limits on $\text{Im } d_t$ ($10^{-16} e cm$) from	
		A_{ch}	A_{fb}	$ A_{ch} $	$ A_{fb} $
0	290	.000	.149		.185
10	286	-.003	.146	9.23	.189
20	273	-.012	.140	2.44	.203
30	252	-.025	.128	1.19	.230
40	221	-.041	.113	.774	.277
50	186	-.057	.095	.599	.362
60	144	-.073	.074	.534	.529
70	98	-.086	.050	.551	.937
80	50	-.094	.026	.706	2.595

Table 3: Limits on $\text{Im } d_t$ of the top quark from the charge asymmetry and the combined asymmetry for different cut-off angles. Helicities of the initial electron and laser beams are $\lambda_e^1 = -.5$, $\lambda_e^2 = -.5$, $\lambda_l^1 = -1$ and $\lambda_l^2 = 1$. A top-quark mass of 174 GeV and an electron beam energy of 250 GeV are used. Laser beam energy is taken to be 1.24 eV, which corresponds to $x = 4.75$. Asymmetries are for $\text{Im } d_t = \frac{1}{2m_t}$.

x	N	Asymmetries		Limits on $\text{Im } d_t$ ($10^{-16} e cm$) from	
		A_{ch}	A_{fb}	$ A_{ch} $	$ A_{fb} $
2.60	1.1	-.004	.034	113	12.8
3.20	28.8	-.011	.072	7.85	1.22
4.74	250.8	-.025	.128	1.20	.230

Table 4: Limits on $\text{Im } d_t$ calculated at different x values for a fixed beam energy $E_b = 250$ GeV and for a cut-off angle of 30° . The top mass is taken to be 174 GeV and the helicities of the initial beams are $\lambda_e^1 = -.5$, $\lambda_{e\gamma}^2 = -.5$, $\lambda_l^1 = -1$ and $\lambda_l^2 = 1$.

that case the sensitivity would be comparable to that obtained in $e^+e^- \rightarrow t\bar{t}$ with $\sqrt{s} = 500$ GeV [3, 5, 6].

For comparison, we mention the result of Baek *et al.* [13] (who have extended the work of [12], and corrected numerical errors therein). They have obtained limits on the real part of the dipole moments of the top quark from a number asymmetry and with linearly polarized photons to be of the order of 10^{-17} *ecm* for a beam energy of 250 GeV.

The sensitivities discussed above are under ideal experimental conditions, which may not be met in practice. A more detailed calculation taking into account experimental cuts and realistic choices of parameters like laser-photon energies, degrees of polarization of the beams, etc. would be important to carry out. However, the results obtained here would be indicative of the possibilities in a realistic case.

The asymmetries we discuss only give limits on the imaginary part of the top EDFF. It would be interesting to study other asymmetries which give limits on the real part of d_t in the presence of circularly polarized photon beams.

Acknowledgement

We thank V. Ravindran for collaboration in the initial stages of the work.

Appendix

A Expressions for $d\sigma_{ij}$ and ξ_2 for $\gamma\gamma \rightarrow X$

Expressions for $d\sigma_{ij}$ and ξ_2 for a general process $\gamma\gamma \rightarrow X$, referred to in eq. (8), are given here in terms of the amplitudes.

$d\sigma_{ij}$ are given by

$$\begin{aligned} d\sigma_{00} &= \frac{1}{4} \sum_{\lambda_\gamma, \lambda'_\gamma} |M(\lambda_\gamma, \lambda'_\gamma)|^2 d\Gamma \\ d\sigma_{22} &= \frac{1}{4} \sum_{\lambda_\gamma, \lambda'_\gamma} \lambda_\gamma \lambda'_\gamma |M(\lambda_\gamma, \lambda'_\gamma)|^2 d\Gamma \\ (d\sigma_{20} + d\sigma_{02}) &= \frac{1}{2} \sum_{\lambda_\gamma} \lambda_\gamma |M(\lambda_\gamma, \lambda_\gamma)|^2 d\Gamma \\ (d\sigma_{20} - d\sigma_{02}) &= \frac{1}{2} \sum_{\lambda_\gamma} \lambda_\gamma |M(\lambda_\gamma, -\lambda_\gamma)|^2 d\Gamma \end{aligned}$$

Helicities of the particles in the final state are summed over, and not shown. $d\Gamma$ is the appropriate phase space factor for the final state X .

The Stokes parameters, ξ_i are given in general by

$$\xi_i = \frac{\Phi_i}{\Phi_0},$$

where $j = 0, 1, 2, 3$ and Φ_i is a function depending on the azimuthal angle, ϕ of the scattered photon beam when initial electron beam is taken along the z axis:

$$\Phi_j = \sum_{n=0}^4 (C_{jn} \cos n\phi + S_{jn} \sin n\phi),$$

where C_{jn} and S_{jn} are certain real coefficients. The circular polarization of the photon arising from Compton scattering, after averaging over the azimuthal angle, is

$$\langle \xi_2 \rangle = C_{20}/C_{00},$$

where

$$\begin{aligned} C_{00} &= \frac{1}{1-y} + 1 - y - 4r(1-r) - 2\lambda_e\lambda_l r x(2r-1)(2-y) \\ C_{20} &= 2\lambda_e r x [1 + (1-y)(2r-1)^2] - \lambda_l(2r-1) \left(\frac{1}{1-y} + 1 - y \right). \end{aligned} \quad (23)$$

A similar expression would hold for the circular polarization $\langle \bar{\xi}_2 \rangle$ of the photon coming from the other beam.

B Density Matrix Elements for $\gamma\gamma \rightarrow t(\lambda_t)\bar{t}(\lambda_{\bar{t}})$

Expressions for ρ_{ij}^{\pm} used in eq. (16) are given below.

$$\begin{aligned} \rho_{00}^+(\lambda_t, \lambda'_t) &= \frac{1}{4} \sum_{\lambda_\gamma, \lambda'_\gamma, \lambda_{\bar{t}}} M(\lambda_\gamma, \lambda'_\gamma, \lambda_t, \lambda_{\bar{t}}) M^*(\lambda_\gamma, \lambda'_\gamma, \lambda'_t, \lambda_{\bar{t}}) \\ \rho_{22}^+(\lambda_t, \lambda'_t) &= \frac{1}{4} \sum_{\lambda_\gamma, \lambda_{\bar{t}}} [M(\lambda_\gamma, \lambda_\gamma, \lambda_t, \lambda_{\bar{t}}) M^*(\lambda_\gamma, \lambda_\gamma, \lambda'_t, \lambda_{\bar{t}}) \\ &\quad - M(\lambda_\gamma, -\lambda_\gamma, \lambda_t, \lambda_{\bar{t}}) M^*(\lambda_\gamma, -\lambda_\gamma, \lambda'_t, \lambda_{\bar{t}})] \\ (\rho_{20}^+(\lambda_t, \lambda'_t) + \rho_{02}^+(\lambda_t, \lambda'_t)) &= \frac{1}{2} \sum_{\lambda_\gamma, \lambda_{\bar{t}}} \lambda_\gamma M(\lambda_\gamma, \lambda_\gamma, \lambda_t, \lambda_{\bar{t}}) M^*(\lambda_\gamma, \lambda_\gamma, \lambda'_t, \lambda_{\bar{t}}) \\ (\rho_{20}^+(\lambda_t, \lambda'_t) - \rho_{02}^+(\lambda_t, \lambda'_t)) &= \frac{1}{2} \sum_{\lambda_\gamma, \lambda_{\bar{t}}} \lambda_\gamma M(\lambda_\gamma, -\lambda_\gamma, \lambda_t, \lambda_{\bar{t}}) M^*(\lambda_\gamma, -\lambda_\gamma, \lambda'_t, \lambda_{\bar{t}}) \\ \\ \rho_{00}^-(\lambda_{\bar{t}}, \lambda'_{\bar{t}}) &= \frac{1}{4} \sum_{\lambda_\gamma, \lambda'_\gamma, \lambda_t} M(\lambda_\gamma, \lambda'_\gamma, \lambda_t, \lambda_{\bar{t}}) M^*(\lambda_\gamma, \lambda'_\gamma, \lambda_t, \lambda'_{\bar{t}}) \\ \rho_{22}^-(\lambda_{\bar{t}}, \lambda'_{\bar{t}}) &= \frac{1}{4} \sum_{\lambda_\gamma, \lambda_t} [M(\lambda_\gamma, \lambda_\gamma, \lambda_t, \lambda_{\bar{t}}) M^*(\lambda_\gamma, \lambda_\gamma, \lambda_t, \lambda'_{\bar{t}}) \\ &\quad - M(\lambda_\gamma, -\lambda_\gamma, \lambda_t, \lambda_{\bar{t}}) M^*(\lambda_\gamma, -\lambda_\gamma, \lambda_t, \lambda'_{\bar{t}})] \\ (\rho_{20}^-(\lambda_{\bar{t}}, \lambda'_{\bar{t}}) + \rho_{02}^-(\lambda_{\bar{t}}, \lambda'_{\bar{t}})) &= \frac{1}{2} \sum_{\lambda_\gamma, \lambda_t} \lambda_\gamma M(\lambda_\gamma, \lambda_\gamma, \lambda_t, \lambda_{\bar{t}}) M^*(\lambda_\gamma, \lambda_\gamma, \lambda_t, \lambda'_{\bar{t}}) \\ (\rho_{20}^-(\lambda_{\bar{t}}, \lambda'_{\bar{t}}) - \rho_{02}^-(\lambda_{\bar{t}}, \lambda'_{\bar{t}})) &= \frac{1}{2} \sum_{\lambda_\gamma, \lambda_t} \lambda_\gamma M(\lambda_\gamma, -\lambda_\gamma, \lambda_t, \lambda_{\bar{t}}) M^*(\lambda_\gamma, -\lambda_\gamma, \lambda_t, \lambda'_{\bar{t}}) \end{aligned}$$

Substituting the amplitudes from eq. (15) we get

$$\begin{aligned}
\rho_{00}^+(\pm, \pm) &= \rho_{00}^-(\pm, \pm) \\
&= \frac{1}{4} C \left\{ \frac{s}{2m_t^2} \left[(1 - \beta_t^4) + A \right] \pm \text{Im } d_t B_0 \right\} \\
\rho_{00}^\pm(+ -) &= -\frac{1}{4} C \frac{s^{3/2} \beta_t}{m_t^2} \text{Im } d_t \sin \theta_t \cos \theta_t \left((1 - \beta_t^2) + \beta_t^2 \sin^2 \theta_t \right) \\
\rho_{22}^+(\pm, \pm) &= \rho_{22}^-(\pm, \pm) \\
&= \frac{1}{4} C \left\{ \frac{s}{2m_t^2} \left[(1 - \beta_t^4) - A \right] \pm \text{Im } d_t B_2 \right\} \\
\rho_{22}^\pm(+ -) &= -\frac{1}{4} C \frac{s^{3/2} \beta_t}{m_t^2} \text{Im } d_t \sin \theta_t \cos \theta_t \left((1 - \beta_t^2) - \beta_t^2 \sin^2 \theta_t \right) \\
\rho_{20}^\pm(\lambda, \lambda) &= \frac{1}{2} C \{ \lambda (2 \beta_t \pm D) + 8m_t \text{Im } d_t \} \\
\rho_{20}^\pm(+ -) &= \mp \frac{1}{2} C \sqrt{s} \left\{ \frac{\beta_t^2}{m_t} \sin^3 \theta_t \right. \\
&\quad \left. + \frac{s\beta_t}{2m_t^2} \text{Re } d_t \sin \theta_t \left((1 - \beta_t^2) \cos \theta_t + \beta_t^2 \sin^2 \theta_t \right) \right\} \\
\rho_{02}^\pm(\lambda, \lambda) &= \frac{1}{2} C \{ \lambda (2 \beta_t \mp D) + 8m_t \text{Im } d_t \} \\
\rho_{02}^\pm(+ -) &= \pm \frac{1}{2} C \sqrt{s} \left\{ \frac{\beta_t^2}{m_t} \sin^3 \theta_t \right. \\
&\quad \left. + \frac{s\beta_t}{2m_t^2} \text{Re } d_t \sin \theta_t \left((1 - \beta_t^2) \cos \theta_t - \beta_t^2 \sin^2 \theta_t \right) \right\}
\end{aligned}$$

where A , B_i , C and D are given by

$$\begin{aligned}
A &= \beta_t^2 \sin^2 \theta_t \left[2 - \beta_t^2 \sin^2 \theta_t \right] \\
B_0 &= \frac{2s\beta_t}{m_t} \left[(2 - \sin^2 \theta_t) (1 - \beta_t^2) - \beta_t^2 \sin^4 \theta_t \right] \\
B_2 &= \frac{2s\beta_t}{m_t} \left[(2 - \sin^2 \theta_t) (1 - \beta_t^2) + \beta_t^2 \sin^4 \theta_t \right] \\
C &= 16 \pi^2 Q_t^4 \alpha^2 \frac{16 m_t^2}{s (1 - \beta_t^2 \cos^2 \theta_t)^2} \\
D &= \frac{s \beta_t^2}{2 m_t^2} \sin^2 \theta_t \cos \theta_t.
\end{aligned}$$

$Q_t = 2/3$ is the charge of the top quark. Note that we have kept only linear terms in d_t assuming that the value of dipole form factor is small and hence that higher order terms can be neglected.

References

- [1] F. Abe *et al.* (CDF Collab.), Phys. Rev. Lett. **74**, 2626 (1995); S. Abachi *et al.* (D0 Collab.), Phys. Rev. Lett. **74**, 2632 (1995).
- [2] W. Bernreuther and P. Overman, Z. Phys. **C 61**, 599 (1994); W. Bernreuther and A. Brandenburg, Phys. Lett. **B 314**, 104 (1993); W. Bernreuther and A. Brandenburg, Phys. Rev. **D 49**, 4481 (1994); A. Soni and R.M. Xu, Phys. Rev. Lett. **69**, 33 (1992); A. Pilaftsis and M. Nowakowski, Int. J. Mod. Phys. **A 9**, 1097 (1994); *ibid.* **A 9**, 5849 (1994) (E); D. Atwood and A. Soni, JLAB-TH-96-14, hep-ph/9607481; A. Das and C. Kao, Phys. Lett. **B 372**, 106 (1996); T. Hasuike *et al.*, TOKUSHIMA-96-04, hep-ph/9611304.
- [3] B. Grzadkowski and Z. Hioki, IFT-07-96, TOKUSHIMA 96-01, hep-ph/9604301; B. Grzadkowski and Z. Hioki, Phys. Lett. **B 391**, 172 (1997).
- [4] J.F. Donoghue and G. Valencia, Phys. Rev. Lett. **58**, 451 (1987); G.L. Kane, G.A. Ladinsky and C.-P. Yuan, Phys. Rev. **D 45**, 124 (1991); T. Arens and L.M. Sehgal, Phys. Rev. **D 50**, 4372 (1994); W. Bernreuther, O. Nachtmann, P. Overmann and T. Schröder, Nucl. Phys. **B 388**, 53 (1992); B. Grzadkowski, Phys. Lett. **B 305**, 384 (1993); D. Chang, W.-Y. Keung and I. Phillips, Nucl. Phys. **B 408**, 286 (1993); *ibid.* **429**, 255 (E) (1994); F. Cuyppers and S.D. Rindani, Phys. Lett. **B 343**, 333 (1995); J. Bernabéu, G. A González-Sprinberg and J. Vidal, FTUV/95-15, IFIC/95-15, in *Perspectives for Electroweak Interactions in e^+e^- Collisions*, Proceedings of the Ringberg Workshop on Electroweak Interaction in e^+e^- Collisions (1995), Ed. B. Kniehl, p. 329; A. Bartl, E. Christova and W. Majerotto, Nucl. Phys. **B 460**, 235 (1996) ; *ibid.*, **B 465**, 365 (1996) (E).
- [5] P. Poulose and S.D. Rindani, Phys. Lett. **B 349**, 379 (1995).
- [6] P. Poulose and S.D. Rindani, Phys. Lett. **B 383**, 212 (1996); Phys. Rev. **D 54**, 4326 (1996).
- [7] C.R. Schmidt, Phys. Lett. **B 293**, 111 (1992); C.R. Schmidt and M.E. Peskin, Phys. Rev. Lett. **69**, 410 (1992); J.P. Ma and A. Brandenburg, Z. Phys. **C 56**, 97 (1992); A. Brandenburg and J.P. Ma, Phys. Lett. **B 298**, 211 (1993); W. Bernreuther and A. Brandenburg, Phys. Rev. **D 49**, 4481 (1994); P. Haberl, O. Nachtmann and A. Wilch, Phys. Rev. **D 53**, 4875 (1996); D. Atwood *et al.*, Phys. Rev. **D 54**, 5412 (1996); B. Grzadkowski and B. Lampe, Warsaw preprint UW-IFT-05-97, hep-ph/9706489.
- [8] I. F. Ginzburg *et al.*, Nucl. Inst. Meth. **205**, 47 (1983).
- [9] I. F. Ginzburg *et al.*, Nucl. Inst. Meth. **219**, 5 (1984); V. Telnov, Nucl. Inst. Meth. **A 355**, 3 (1995).
- [10] H. Anlauf, W. Bernreuther and A. Brandenburg, Phys. Rev. **D 52**, 3803 (1995).
- [11] W. Bernreuther, A. Brandenburg and P. Overmann, hep-ph/9602273, PITHA-96-02.

- [12] S.Y. Choi and K. Hagiwara, Phys. Lett. **B 359**, 369 (1995).
- [13] M.S. Baek, S.Y. Choi and C.S. Kim, YUMS 97-7, SNUTP 97-035, hep-ph/9704312.
- [14] S. Y. Tsai, Phys. Rev. **D4**, 2821 (1971); S. Kawasaki, T. Shirafuji and S. Y. Tsai, Prog. Theor. Phys. **49**, 1656 (1973);
- [15] T. Arens and L. M. Sehgal, Nucl. Phys. **B 393**, 46 (1993).
- [16] R. Vega and J. Wudka, Phys. Rev. **D 53**, 5286 (1996).